The EMBO Journal (2013) 32, 2994–3007
www.embojournal.org

SOURCE DATA | TRANSPARENT PROCESS

THE EMBO JOURNAL

REST/NRSF-mediated intrinsic homeostasis protects neuronal networks from hyperexcitability

Davide Pozzi[1,2,4,5], Gabriele Lignani[1,3,4], Enrico Ferrea[1,6], Andrea Contestabile[1], Francesco Paonessa[1], Rosalba D'Alessandro[2], Pellegrino Lippiello[1], Davide Boido[2], Anna Fassio[1,3], Jacopo Meldolesi[2], Flavia Valtorta[2], Fabio Benfenati[1,3] and Pietro Baldelli[1,3,*]

[1]Department of Neuroscience and Brain Technologies, Istituto Italiano di Tecnologia, Genova, Italy, [2]Department of Neuroscience, San Raffaele Scientific Institute, Vita Salute University, Milano, Italy and [3]Department of Experimental Medicine, University of Genova, Genova, Italy

Intrinsic homeostasis enables neuronal circuits to maintain activity levels within an appropriate range by modulating neuronal voltage-gated conductances, but the signalling pathways involved in this process are largely unknown. We characterized the process of intrinsic homeostasis induced by sustained electrical activity in cultured hippocampal neurons based on the activation of the Repressor Element-1 Silencing Transcription Factor/Neuron-Restrictive Silencer Factor (REST/NRSF). We showed that 4-aminopyridine-induced hyperactivity enhances the expression of REST/NRSF, which in turn, reduces the expression of voltage-gated Na^+ channels, thereby decreasing the neuronal Na^+ current density. This mechanism plays an important role in the downregulation of the firing activity at the single-cell level, re-establishing a physiological spiking activity in the entire neuronal network. Conversely, interfering with REST/NRSF expression impaired this homeostatic response. Our results identify REST/NRSF as a critical factor linking neuronal activity to the activation of intrinsic homeostasis and restoring a physiological level of activity in the entire neuronal network.

The EMBO Journal (2013) **32,** 2994–3007. doi:10.1038/emboj.2013.231; Published online 22 October 2013
Subject Categories: neuroscience
Keywords: 4-aminopyridine; excitability; intrinsic homeostasis; Na^+ channels; transcriptional repression

*Corresponding author. Department of Experimental Medicine, University of Genova, Viale Benedetto XV, n 3, Genova 16132, Italy. Tel.: +39 010 353 8191; Fax: +39 010 353 8194;
E-mail: pietro.baldelli@unige.it
[4]These authors contributed equally to this work.
[5]Present address: Laboratory of Pharmacology, Brain Pathology Humanitas Clinical and Research Center, Via Manzoni 113, 20089 Milano, Italy.
[6]Present address: Cognitive Neuroscience Laboratory, German Primate Center, Leibniz Institute for Primate Research, Göttingen, Germany.

Received: 28 February 2013; accepted: 24 September 2013; published online: 22 October 2013

Introduction

Homeostatic plasticity takes place in neurons upon the long-term perturbation of neuronal network activity. By adjusting both the *synaptic strength* (synaptic homeostasis) and the *firing properties* (intrinsic homeostasis), this compensatory mechanism is fundamental to maintain an appropriate operating range in the network (Turrigiano, 2011). *Synaptic* homeostasis, also known as synaptic scaling, has been intensively investigated and has been found to consist of coordinated molecular and functional adjustments of both the presynaptic and the postsynaptic compartments (Turrigiano, 2008; Pozo and Goda, 2010). *Intrinsic* homeostasis, based on the modulation of membrane excitability, has been mostly investigated during prolonged silencing of neuronal activity, in which case it results in an elevated neuronal excitability through adjustments in voltage-dependent conductances (Desai *et al*, 1999; Aptowicz *et al*, 2004; Kuba *et al*, 2010). The opposite form of intrinsic homeostasis, recently reported to develop when dissociated hippocampal cultures are exposed to chronic hyperexcitation (Burrone and Murthy, 2003; Grubb and Burrone, 2010; O'Leary *et al*, 2010), is still poorly understood. In particular, the mechanistic link between prolonged hyperexcitation and the activation of the homeostatic response remains largely undefined.

The Repressor Element-1 Silencing Transcription Factor/Neuron-Restrictive Silencer Factor (REST/NRSF) is a transcriptional repressor known to play a key role in neuronal differentiation (Chong *et al*, 1995; Schoenherr and Anderson, 1995b). The reduction in REST/NRSF expression from the high levels in stem cells, which takes place during the transition from progenitors to mature neurons, increases the expression of many neuron-specific genes bearing the REST/NRSF binding sequence RE-1 in their promoter region. Through this mechanism, REST/NRSF is believed to orchestrate a variety of processes that are critical for neuronal differentiation, including neurogenesis, synaptogenesis, excitability, and synaptic transmission (Ballas and Mandel, 2005; Ooi and Wood, 2007; D'Alessandro *et al*, 2009). In apparent agreement with these data, increases in REST/NRSF induced in mature neurons by the glutamatergic agonist kainate (Palm *et al*, 1998; Spencer *et al*, 2006) or by ischaemic insults (Calderone *et al*, 2003; Formisano *et al*, 2007; Noh *et al*, 2012) are followed by a decreased expression of neuron-specific genes and neurodegeneration. Therefore, increased REST/NRSF levels have been often considered as harmful in mature neurons.

In contrast, we demonstrate that REST/NRSF expression induced in mature hippocampal neurons by prolonged treatment with the stimulatory agent 4-aminopyridine (4AP) is a protective mechanism that governs the inhibitory homeostatic control of intrinsic excitability. Indeed, we found that activity-dependent REST/NRSF expression triggers a homeostatic downregulation of voltage-gated Na^+ (VGNa) channels and currents that allows neurons to readjust the network firing activity at a physiological set point.

Results

Increased spontaneous activity of neuronal networks induced by chronic 4AP triggers homeostatic plasticity

To investigate the effects of increased network activity, we used mature mouse hippocampal neurons treated for 24, 48, and 96 h with the K^+ channel blocker 4AP (100 μM) or with vehicle. Long-term changes in the global network activity were first investigated by measuring $[Ca^{2+}]_i$ transients occurring spontaneously in the neuronal cell body after the removal of 4AP (Figure 1A and B). Compared to parallel 'sister' cultures treated with vehicle only, the whole population of neurons treated with 4AP for 24 h exhibited increases in both the amplitude and the frequency of spontaneous $[Ca^{2+}]_i$ transients. At 48 h of 4AP treatment, however, this enhanced activity was reduced, reaching values comparable to resting levels at 96 h of treatment (Figure 1C).

The long-term effects of 4AP on the entire neuronal network were investigated with microelectrode array (MEA) recordings from 20 to 24 div (Figure 1D). At rest, the extracellularly recorded activity consisted of isolated spikes and network bursts (Figure 1E), as previously shown (Vajda *et al*, 2008). After 24 h in 4AP, the networks displayed much higher spiking rates, which were dramatically decreased after 48 h and returned to basal values after 96 h of treatment (Figure 1F). When the medium collected from neuronal cultures that had been incubated with 4AP for 96 h was added to control cultures, it induced closely similar responses to those induced by fresh 4AP, indicating that the reduction in activity was not due to a loss of 4AP efficacy (Supplementary Figure S1). We conclude that the early state of hyperexcitation induced by 4AP, revealed by increased firing and $[Ca^{2+}]_i$ transients at 24 h, is transient and followed by a return to basal activity at later stages (48 and 96 h), indicating the establishment of a neuronal homeostatic response.

The homeostatic response induced by chronic 4AP reduces neuronal intrinsic excitability through the downregulation of Na^+ channels

To investigate the mechanisms of the homeostatic response at the cellular level, single-cell neuronal excitability was analysed by patch-clamp recordings in the current-clamp configuration by delivering constant current pulses of increasing amplitude and measuring the resulting action potential firing in visually identified excitatory pyramidal neurons (Figure 2A). Upon 96 h of 4AP treatment, the instantaneous frequency versus injected current curve revealed a marked downregulation of the firing activity (Figure 2B) that paralleled the strong reduction in the mean firing frequency (Figure 2C). The shape of the first action potential evoked by current injection (Figure 2D) was analysed using the plot of the time derivative of voltage (dV/dt) versus voltage (Figure 2E). Ninety-six hours in 4AP also reduced the action potential maximum rising slope (Figure 2F) and peak (Figure 2G), whereas the voltage threshold (Figure 2H) and

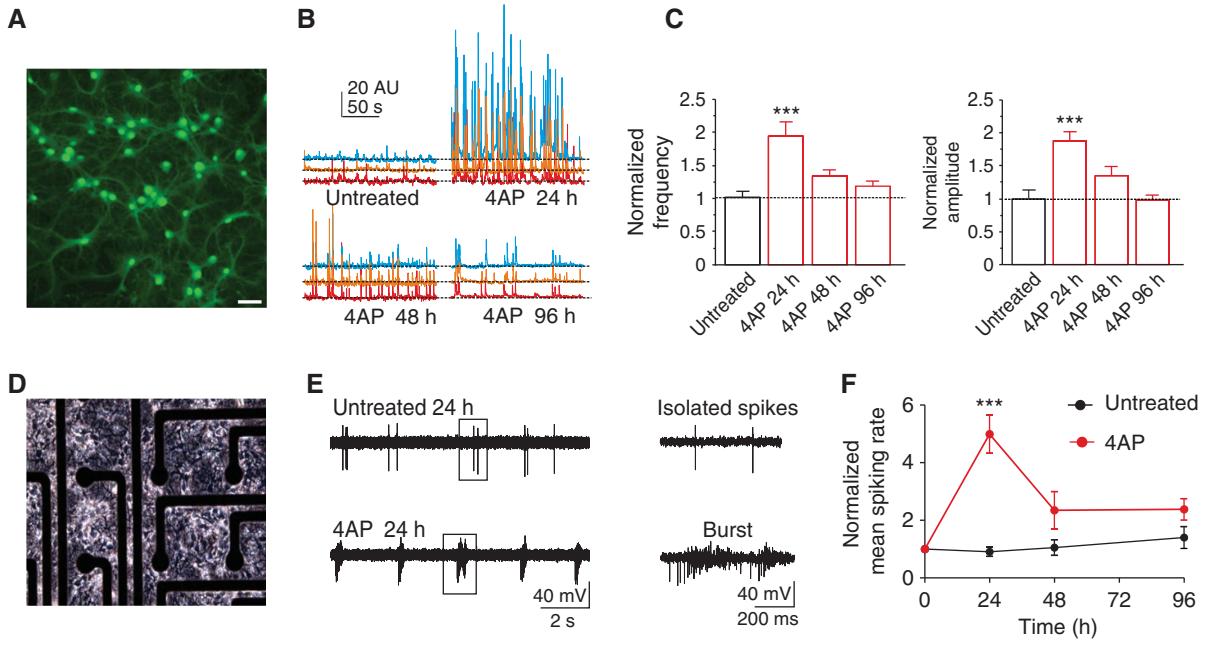

Figure 1 The initially elevated network activity induced by long-term 4AP treatment spontaneously returns to resting levels. (**A**) Representative microphotograph of Oregon green-loaded cultured hippocampal neurons (16 div). Scale bar: 30 μm. (**B**) Representative traces of spontaneous Ca^{2+} rises, as revealed by increases in Oregon green fluorescence, recorded at three neuronal somata incubated in the absence or presence of 4AP for 24, 48, and 96 h. (**C**) Normalized mean (± s.e.m.) frequency (*left*) and amplitude (*right*) of spontaneous Ca^{2+} rises recorded at 18 div in untreated neurons (black bars; $n=23$) or in neurons treated for 24 ($n=22$), 48 ($n=22$), and 96 h ($n=62$) with 4AP (red bars). $^{***}P<0.001$ (one-way ANOVA followed by the Bonferroni's test). (**D**) Representative microphotograph of hippocampal cultures (20 div) plated on an MEA chip. Electrode diameter, 30 μm. (**E**) Representative voltage traces recorded from cultured neurons incubated for 24 h in the absence (*top*) or presence (*bottom*) of 4AP showing single spike and bursting activities, respectively. Close-ups of the voltage traces are shown on the right. (**F**) Time course of the normalized (mean ± s.e.m.) spiking rate for neuronal cultures incubated for 24, 48, and 96 h in the absence (black line/symbols) or presence (red line/symbols) of 4AP. Each culture was recorded over time and the data were normalized for the respective basal value recorded before the 4AP treatment. The mean spiking rate was transiently enhanced by 4AP treatment for 24 h ($^{***}P<0.001$, Friedman's two-way ANOVA followed by Dunn's multiple comparison test; $n=8$ for untreated and $n=6$ for 4AP-treated networks), but the effect was lost after 48 and 96 h of 4AP treatment.

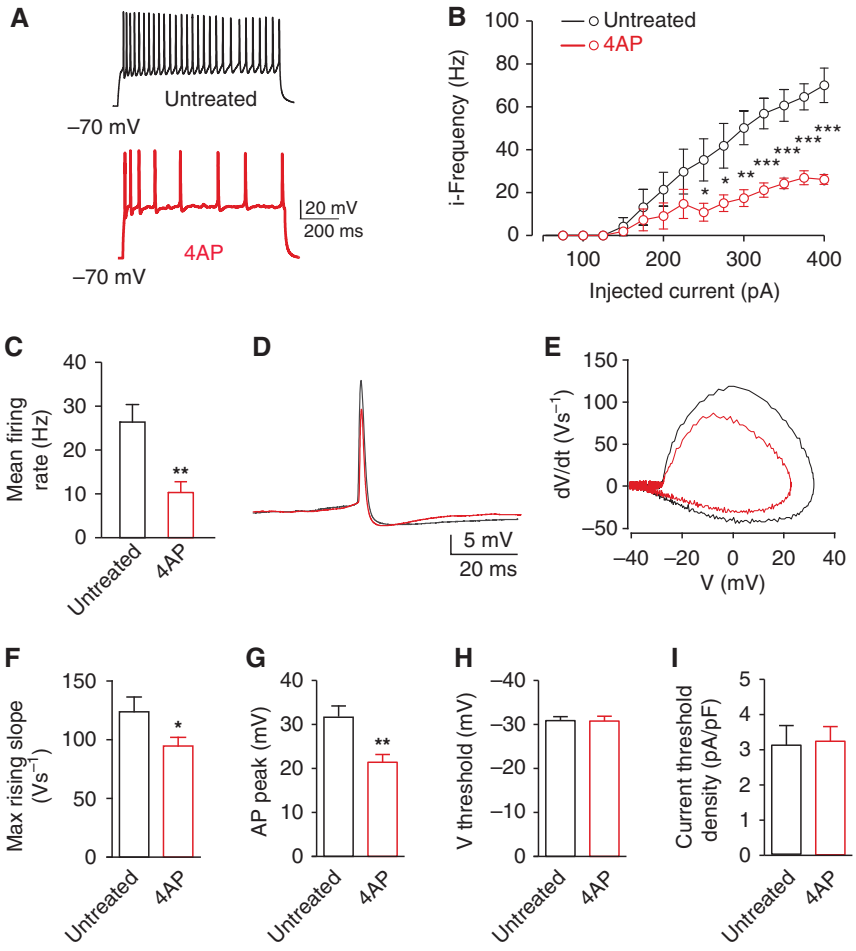

Figure 2 Long-term 4AP treatment reduces neuronal excitability at the single-cell level. (**A**) Representative current-clamp recordings of spike trains evoked by somatic current injection under control conditions or after 4AP treatment for 96 h. All current-clamp experiments were performed on neurons with a pyramidal morphology in the presence of synaptic transmission blockers (for details, see Materials and methods). Mean instantaneous frequency versus injected current relationship (iF/I curve) (**B**) and mean firing frequency (**C**) measured either in untreated neurons (black symbols; $n = 17$) or in neurons treated with 4AP for 96 h (red symbols; $n = 17$). Representative traces of action potential (**D**) and phase-plane plot (**E**) are shown. (**F–I**) The mean (± s.e.m.) maximum rising slope (**F**), action potential peak (**G**), V threshold (**H**) and current threshold density (**I**) calculated either in untreated neurons (black bars; $n = 14$) or in neurons treated with 4AP for 96 h (red bars; $n = 19$) as described in Materials and methods and Supplementary Table S1. The mean maximum rising slope and action potential peak were significantly decreased by treatment with 4AP for 96 h (*$P < 0.05$, **$P < 0.01$, Student's unpaired two-tailed *t*-test).

the current threshold density (Figure 2I) were unchanged. Additional electrophysiological parameters including capacitance, action potential after hyperpolarization, and input resistance were also unchanged (see Supplementary Table S1). These data indicate that the activation of a homeostatic response, induced by long-term hyperactivity, reduces neuronal excitability.

The intrinsic neuronal excitability is tightly dependent on the activity of several ion channels. The reduction in the maximum rising slope and peak of the action potential (Figure 2F and G) observed upon 96 h of 4AP treatment strongly suggested the presence of a negative modulation of the VGNa channels, which predominates in the early phase of the action potential (Henze and Buzsaki, 2001). To evaluate the amplitude of the overall Na^+ current density (I_{Na}) in treated cells, we used cell-attached macro-patch recordings, a technique that is not subject to space-clamp errors (Figure 3A and B; Magistretti *et al*, 1999).

Membrane patches on the somata of cultured hippocampal pyramidal neurons, initially clamped at − 100 mV, were depolarized by delivering a series of voltage steps between − 60 and + 60 mV in 10 mV increments (Figure 3B), and the maximum Na^+ current amplitude (I_{Na}) at each potential was normalized to the patched membrane area (Figure 3C). When neuronal cultures incubated in the presence of 4AP for 96 h were analysed, a significant reduction in I_{Na} density evoked by depolarization in the − 10/0 mV range was observed compared to sister cultures treated with vehicle (Figure 3C). In contrast, the activation and inactivation of VGNa currents were substantially unaffected (Figure 3D; Supplementary Figure S2), indicating that the I_{Na} reduction was not due to a change in the biophysical properties of the channels but, rather, to a decrease in their membrane expression induced by the 4AP treatment.

Furthermore, if a downregulation of VGNa channels was really responsible for the reduced neuronal excitability, then their partial inactivation should mimic the effect observed upon chronic 4AP treatment. Indeed, sub-saturating concentrations of tetrodotoxin (TTX) had effects on the firing frequency similar to those observed upon 4AP stimulation (Supplementary Figure S3).

The estimated half-life of VGNa channels is ~1–2 days (Schmidt and Catterall, 1986). Thus, the 96-h treatment with

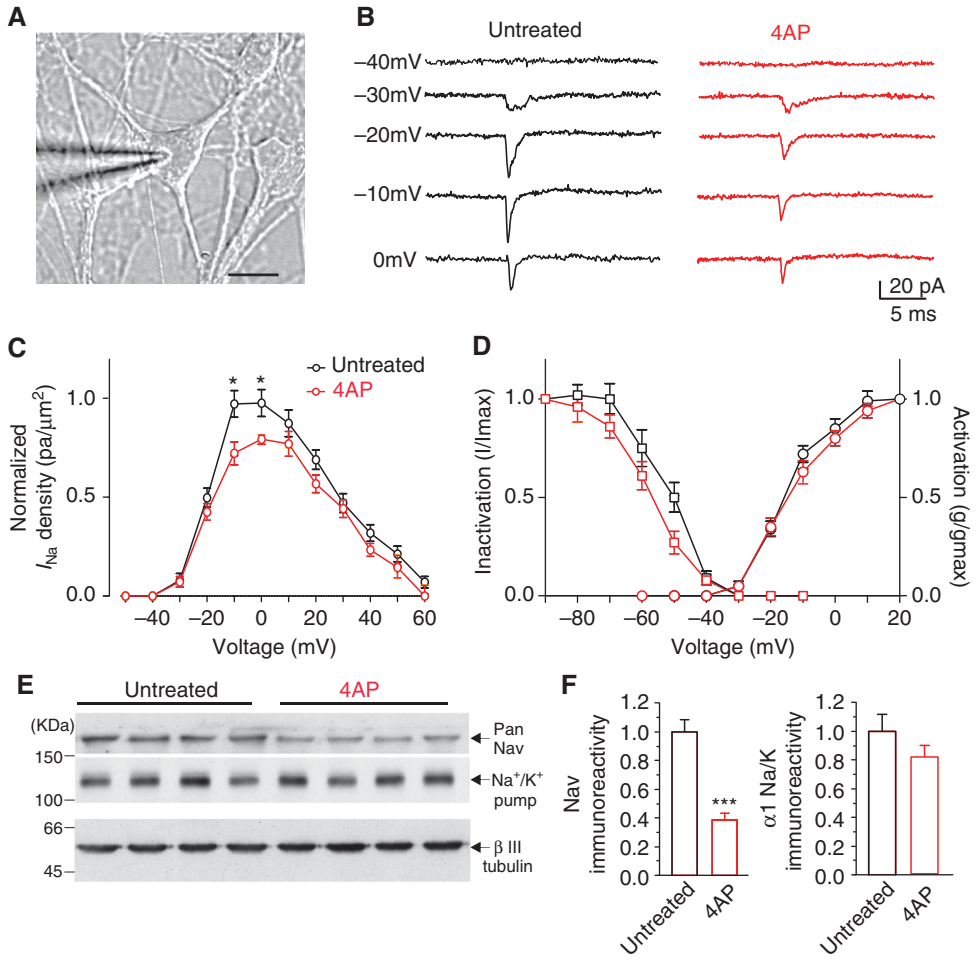

Figure 3 VGNa channels are downregulated upon long-term 4AP treatment. (**A**) Representative microphotograph of a patched pyramidal hippocampal neuron (16 div). Scale bar: 15 µm. (**B**) Representative I_{Na} traces obtained in cell-attached configuration at various voltages and recorded in untreated neurons (black traces) or in neurons treated with 4AP for 96 h (red traces). (**C**) Plots of the mean (± s.e.m.) I_{Na} normalized to the maximum amplitude versus voltage for untreated (black; $n = 34$) and 4AP-treated (4AP 96 h, red; $n = 20$) neurons. $^*P < 0.05$; Student's unpaired two-tailed *t*-test with Welch's correction for non-equal variance. (**D**) Mean I_{Na} current activation (dots) and inactivation (squares) curves for untreated (black, $n = 34$) and 4AP-treated (red, $n = 20$) cells. The inactivation curve was fitted using a Boltzmann equation as described in Materials and methods and shown in Supplementary Figure S2. (**E**) Protein expression levels of VGNa channels (Pan-Nav) and α1 subunits of the Na^+/K^+ pump evaluated by western blot analysis in untreated or 4AP-treated hippocampal neurons. Five distinct samples are shown for each experimental group. (**F**) Immunoreactive bands for VGNa channels (*left*) and Na^+/K^+ pump (*right*) were quantified and normalized to the β-III tubulin signal (see Materials and methods). VGNa channel expression was significantly decreased after 96 h of 4AP treatment ($^{***}P < 0.001$, Student's unpaired two-tailed *t*-test ($n = 12$, from three independent cell-culture preparations). Source data for this figure is available on the online supplementary information page.

4AP may be long enough to induce significant reductions in the levels of the channel proteins. To investigate this possibility, untreated and 4AP-treated hippocampal cultures were analysed by western blotting using an anti-pan-VGNa channel antibody (Figure 3E and F). Upon 96 h of 4AP treatment, the levels of VGNa channels were decreased by over 50%, whereas the levels of the α1 subunit of the Na^+/K^+ pump, another abundant plasma membrane protein, were unaffected (Figure 3E and F). The large reduction in the VGNa channel levels induced by prolonged stimulation may therefore play a critical role in the homeostatic response affecting the intrinsic neuronal excitability.

Increased neuronal network activity enhances the expression of REST/NRSF. The downregulation of VGNa channels observed upon long-term 4AP treatment might result from various mechanisms operating at the transcriptional and/or post-transcriptional level. The expression of type II VGNa channel (Nav1.2), long known as REST/NRSF target (Chong *et al*, 1995), has been shown to undergo silencing upon increases in REST/NRSF levels in both neurons (Nadeau and Lester, 2002) and PC12 cells (Ballas *et al*, 2001). These findings suggested us to investigate whether the changes in Nav1.2 levels in response to long-term 4AP treatment were induced by upstream changes in REST/NRSF expression.

Before studying the responses of REST/NRSF and Nav1.2 expression to hyperactivity, we investigated by qRT–PCR analysis whether the *in vitro* development of the neuronal network from 12 to 25 div was associated with endogeneous changes in REST/NRSF and Nav1.2 mRNA levels. We found that REST/NRSF mRNA levels, constant during the early stages of *in vitro* maturation, increased between 15 and 20 div to reach a steady-state level (Supplementary Figure S4a). Over a similar time window, the Nav1.2 mRNA was also upregulated (Supplementary Figure S4b). These temporal profiles indicate that Nav1.2 expression during this develop-

mental phase is regulated by several factors and that the parallel changes in REST/NRSF and Nav 1.2 mRNAs are likely the expression of a general maturation of the network.

Next, we investigated the changes in the expression levels of REST/NRSF and Nav1.2 at various time points after the application of 4AP (Figure 4A and B). Remarkably, the REST/NRSF mRNA displayed a significant increase after 8 h, peaked at 24 h, remained high up to 48 h and returned to basal levels at 96 h (Figure 4A). This increase in the REST/NSRF transcript was precisely mirrored by a parallel, significant reduction in the levels of Nav1.2 mRNA that was already apparent at 8 h after 4AP application and persisted for up to 24 h (Figure 4B). The REST/NRSF mRNA is translated into an endogeneous protein that migrates at ~195 kDa in western blots (Rodenas-Ruano *et al*, 2012), as shown by the electrophoretic mobility of recombinant REST/NRSF expressed in the SH-SY5Y neuroblastoma cell line (Figure 4C and the scanned full-length blot in Supplementary Figure S5). Western blot analysis of cortical neurons, performed at various time points after the application of 4AP, revealed that the transient rise of REST/NRSF transcription was paralleled by a marked and progressive increase in the expression of the endogeneous protein at 24, 48, and 96 h of treatment with 4AP (Figure 4C and D).

In previous studies, increases in REST/NRSF induced by treatment with the glutamatergic analogue kainate or ischaemia were reported to be a cause of neuronal death (Calderone *et al*, 2003; Spencer *et al*, 2006). To determine whether this also occurred in hippocampal cultures chronically treated with 4AP, a neuronal viability assay with propidium iodide was carried out (Figure 4E and F). We found that the small percentage of dead neurons found in untreated cultures (~7%) was unchanged in cultures treated with 4AP for 24, 48, or 96 h (Figure 4E and F). These data are also supported by the evidence that the passive membrane properties of both control and 4AP-treated neurons were totally unaltered (Supplementary Table S1). In contrast, the percentage of dead neurons was much higher (~50%) in cultures treated

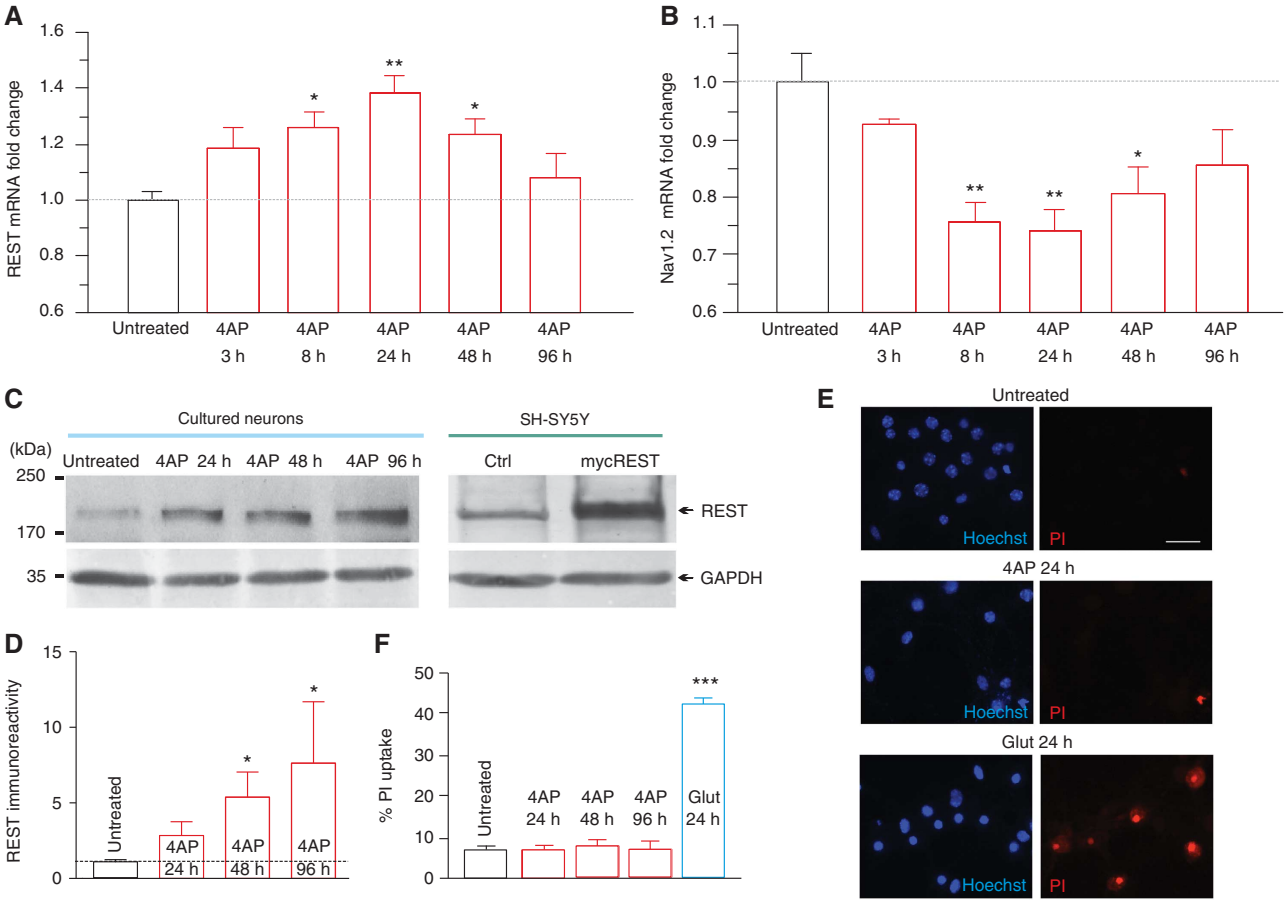

Figure 4 Neuronal activity increases the REST/NRSF expression without inducing cell death. (**A**, **B**) qRT-PCR analysis of changes (means ± s.e.m.) in REST/NRSF and Nav1.2 mRNA transcript levels in untreated or 4AP-treated cortical neurons (*$P<0.05$, **$P<0.01$, Kruskal–Wallis's followed by the Dunn's test versus untreated). For each time point, $n=7$–8 from two independent neuronal preparations. (**C**) Representative western blot analysis from cultured cortical neurons, either untreated or treated with 4AP at the indicated times, showing the expression of REST/NRSF and GAPDH proteins. The molecular weight of REST/NRSF in SDS–PAGE (≈195 KDa) was confirmed by immunoblotting (right) in SH-SY5Y neuroblastoma cells transfected with either the empty (ctrl) or the REST/NRSF expression vector (mycREST). (**D**) Quantification of REST/NRSF protein. All values were normalized to the untreated levels (*$P<0.05$, Kruskal–Wallis's followed by the Dunn's test versus untreated; $n=4$). (**E**) Representative images of cell-death analysis performed in untreated neurons and in neurons treated with either 4AP for 24, 48 and 96 h or glutamate for 24 h. Total neurons were stained with the cell-permeable Hoechst dye (blue), whereas dead cells were identified with propidium iodide staining (red). Scale bar: 100 μm. (**F**) Quantification of the propidium iodide-positive cells expressed in the percentage of the number of Hoechst-positive cells. Data are means ± s.e.m. (***$P<0.001$ versus untreated, one-way ANOVA followed by the Bonferroni's test; $n=20$ for each condition from three independent preparations).

with glutamate for 24 h (Figure 4E and F). The dissociation between the similar increases in REST/NRSF induced by 4AP and glutamate and their quite different effects on neuronal viability excludes the possibility that an increase in REST/NRSF levels *per se* can promote neuronal death.

Exogeneous expression of REST/NRSF in neurons reduces their intrinsic excitability

To explore the functional role of REST/NRSF in neurons, 16 div hippocampal neurons were transiently co-transfected with two plasmids encoding for a myc-tagged REST/NRSF and for GFP, respectively. Four days later, virtually all GFP-positive neurons exhibited strong myc signals in the nucleus, demonstrating the expression and correct localization of the transfected REST/NRSF (Figure 5A).

When short tetanic field stimulations (40 APs at 20 Hz) were applied to resting cultured neurons (16 div) loaded with the ratiometric dye Fura-2 in the presence of synaptic transmission blockers (CNQX, AP-5, bicuculline, CGP), rapid cell body $[Ca^{2+}]_i$ transients blocked by TTX were triggered with fast mono-exponential decays (time constant: 5.0 ± 0.4 s) (Supplementary Figure S6). When GFP + mycREST-positive neurons were stimulated, their fast $[Ca^{2+}]_i$ transients were significantly smaller than those of non-transfected neurons or

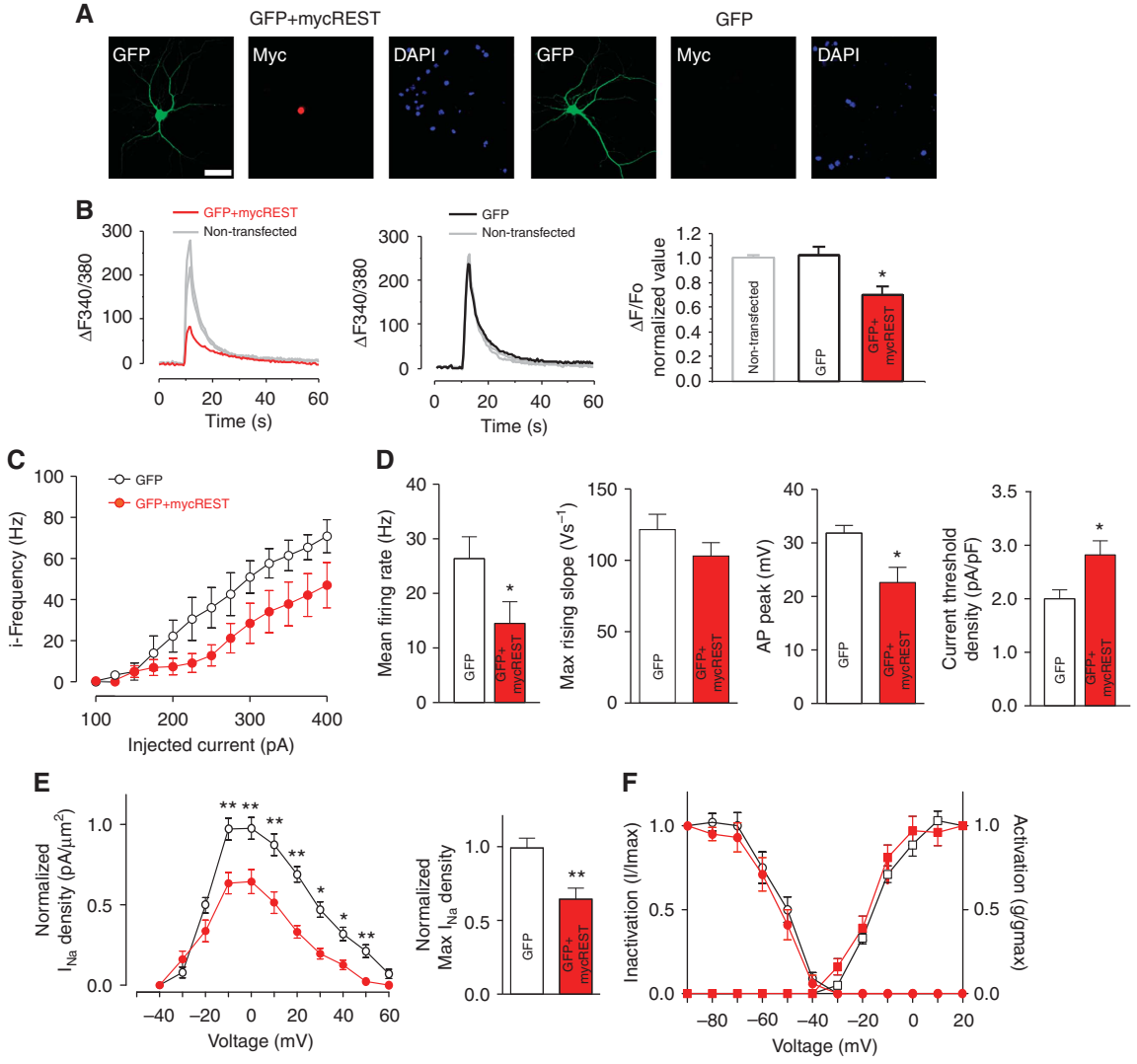

Figure 5 Overexpression of REST/NRSF reduces neuronal excitability and I_{Na} current density. (**A**) Representative images of hippocampal neurons (16 div) co-transfected with GFP together with either a myc-tagged REST/NRSF expression vector (GFP + mycREST; *left panels*) or an empty vector (GFP; *right panels*). From left to right: GFP fluorescence (green), myc immunoreactivity (red), and DAPI staining (blue). Scale bar: 25 μm. (**B**) (*Left panels*) Representative traces of electrically evoked Ca^{2+} transients recorded at the cell body of non-transfected neurons (grey traces) or of neurons expressing either GFP alone (black trace) or GFP + mycREST (red trace). (*Right panel*) Quantitative analysis of the evoked Ca^{2+} influx recorded in non-transfected neurons ($n = 30$) or in neurons expressing either GFP alone ($n = 17$) or GFP + MycREST ($n = 18$) (*$P < 0.05$, GFP + MycREST versus GFP + empty vector; one-way ANOVA followed by the Bonferroni's test). (**C**) Plots of the mean instantaneous frequency versus injected current (iF/I curve) for pyramidal neurons expressing either GFP alone (black) or GFP + mycREST (red) ($n = 16$). (**D**) Mean (± s.e.m.) firing rate, maximum rising slope, action potential peak, and current threshold density. Significant changes were observed in the firing rate, action potential peak, and current threshold density of GFP + mycREST versus GFP-expressing neurons (*$P < 0.05$, Student's unpaired two-tailed *t*-test; $n = 16$). (**E**) (*Left*) Mean (± s.e.m.) normalized I_{Na} density versus voltage measured in hippocampal pyramidal neurons expressing either GFP alone (black, $n = 30$) or GFP + mycREST (red, $n = 16$). A significant decrease in the I_{Na} density was observed in GFP + mycREST-expressing neurons (*$P < 0.05$, **$P < 0.01$, Student's unpaired two-tailed *t*-test with Welch's correction). (**F**) Average I_{Na} activation (squares) and inactivation (circles) curves for neurons expression either GFP (empty symbols, $n = 30$) or GFP + mycREST (red symbols; $n = 16$).

of neurons transfected with the GFP vector alone (Figure 5B), suggesting a role for REST/NRSF in the control of neuronal excitability.

We then measured the firing rate in hippocampal pyramidal neurons in which REST/NRSF expression had been increased. The relationship between average instantaneous frequency and injected current, measured by parallel patch-clamp experiments, was right shifted in REST/NRSF-transfected neurons as compared to neurons transfected with the empty vector (Figure 5C). Neurons overexpressing REST/NRSF displayed a greatly reduced mean firing rate and action potential peak and an increased current threshold density (Figure 5D), but no change in the maximum rising slope (Figure 5D) and in the V threshold (GFP: -29.57 ± 2.5 mV, $n = 16$; REST/NRSF-myc: -29.08 ± 2.4 mV, $n = 16$). The reduction in the neuronal firing rate was associated with a significant decrease in I_{Na} revealed by macro-patch recordings (Figure 5E). In contrast, the activation and inactivation curves of somatic Na^+ currents were virtually unaffected (Figure 5F). Taken together, these results demonstrate that REST/NRSF plays a major role in the control of neuronal excitability of hippocampal pyramidal neurons.

Exogeneous expression of REST/NRSF downregulates VGNa channels and downregulates the firing activity of the whole neuronal network

To investigate the global effects of REST/NRSF on neuronal network activity, we switched from transfection to infection of hippocampal cultures using lentiviruses expressing either mycREST/NRSF together with GFP or GFP alone. Virtually all neurons of the cultures infected with lentiviruses expressing GFP and mycREST/NRSF were strongly labelled for the transcription factor (Figure 6A) and displayed REST/NRSF mRNA levels 7.01 ± 0.9-fold higher than control GFP-infected neurons ($n = 3$, $P < 0.01$). Consistent with the results described above (Figure 5C–F), the levels of VGNa channels, measured in the cultures by western blotting, were reduced by $\sim 75\%$ in the REST/NRSF-infected cultures (Figure 6B).

The overall network firing activity, assayed by MEA recordings, exhibited considerable changes over time in culture. During the first 7 days post infection (12–18 div), the physiological, developmentally regulated, increase in the spiking rate in control and REST/NRSF-expressing networks almost coincided. During the following 7 days (19–25 div), however, the spiking rates of control networks continued to increase, whereas those of the REST/NRSF-infected networks remained fairly constant (Figure 6C–E). The electrical activity recorded in the networks is mostly due to collective events known as 'network bursts' (Figure 6C and D). The data were thus further analysed by calculating the time-dependent changes in the mean rates and duration of the bursts. The dramatic impairment in the build-up of the firing rate during *in vitro* development observed in the high REST/NRSF cultures was entirely due to a parallel decrease in bursting rate (Figure 6F), whereas no changes were observed in burst duration (Figure 6G).

Endogeneous REST/NRSF participates in the establishment of intrinsic homeostasis following neuronal hyperactivity

The repression of both single-neuron and neuronal network excitability induced by REST/NRSF overexpression (see Figures 5 and 6) is reminiscent of what occurring during long-term treatment with 4AP (see Figures 1 and 2), a condition that increases the endogeneous REST/NRSF levels (see Figure 4). To investigate whether a causal link exists between high REST/NRSF expression and the homeostatic reduction in the 4AP-induced hyperexcitability, we employed two REST/NRSF-specific shRNAs (#1 and #2) that were assessed to be effective in downregulating both the exogeneously expressed and the endogeneous REST/NRSF levels in both cell lines and primary neurons (Supplementary Figure S7a–c; Tomasoni *et al*, 2011).

To explore whether the developmental increase in endogeneous network activity (Figure 6E–G) is dependent on the altered REST/NRSF levels, we first monitored neuronal network activity in cultures infected with either scrambled shRNA or REST/NSRF-specific shRNA#1 by using MEA recordings. No effects on the age-dependent increase in spontaneous firing were found upon downregulation of the endogeneous REST/NRSF levels (Supplementary Figure S7d).

We then investigated the excitability of neurons transfected with either shRNA#1, shRNA#2 or a scrambled shRNA after 96 h treatment with 4AP, a time point at which spontaneous Ca^{2+} waves (Figure 1C), firing activity (Figure 1F) and electrically evoked $[Ca^{2+}]_i$ transients (Supplementary Figure S6c) had returned to control values. Strikingly, in neurons transfected with shRNA#1, but not with the scrambled shRNA, such homeostatic responses were absent. Specifically, the amplitude of the electrically evoked $[Ca^{2+}]_i$ responses (Figure 7A), neuronal firing rate (Figure 7B and C), maximum rising slope (Figure 7D), action potential peak (Figure 7E), current threshold density (Figure 7F), and I_{Na} density (Figure 7G and H), revealed the persistence of a state of hyperexcitability as compared to 4AP-treated neurons expressing the scrambled shRNA. Interestingly, in the absence of 4AP treatment none of these parameters were affected by transfection with shRNA#1. Similar results were obtained in neurons transfected with shRNA#2 (Supplementary Figure S8). Taken together, these data strongly suggest that the observed changes in intrinsic excitability and VGNa channel activity during long-term treatment with 4AP are largely mediated by the increases in REST/NRSF levels.

Physiological activity of the whole neuronal network is restored by the REST/NRSF-mediated homeostatic plasticity

To extend these findings to the entire neuronal network, lentiviruses encoding either scrambled or the REST/NRSF-specific shRNAs were employed to infect the majority of neurons grown onto MEA chips to test the spontaneous network activity upon long-term 4AP treatment (24, 48, and 96 h; Figure 8A).

While non-infected neurons (20 div) and neurons infected with either scrambled shRNA or shRNA#1/#2 displayed very similar spontaneous firing rates under control conditions (Figure 8B–D, upper panels), significant differences took place upon long-term 4AP treatment (96 h; Figure 8C and D, lower panels). In the cultures infected with the scrambled shRNA, the responses were similar to those observed in control cells (see Figure 1E and F), with an initial phase of hyperexcitation at 24 h, followed by a progressive reduction in both spiking and bursting rates at 48 and 96 h, to levels similar to those of parallel cultures not treated with 4AP

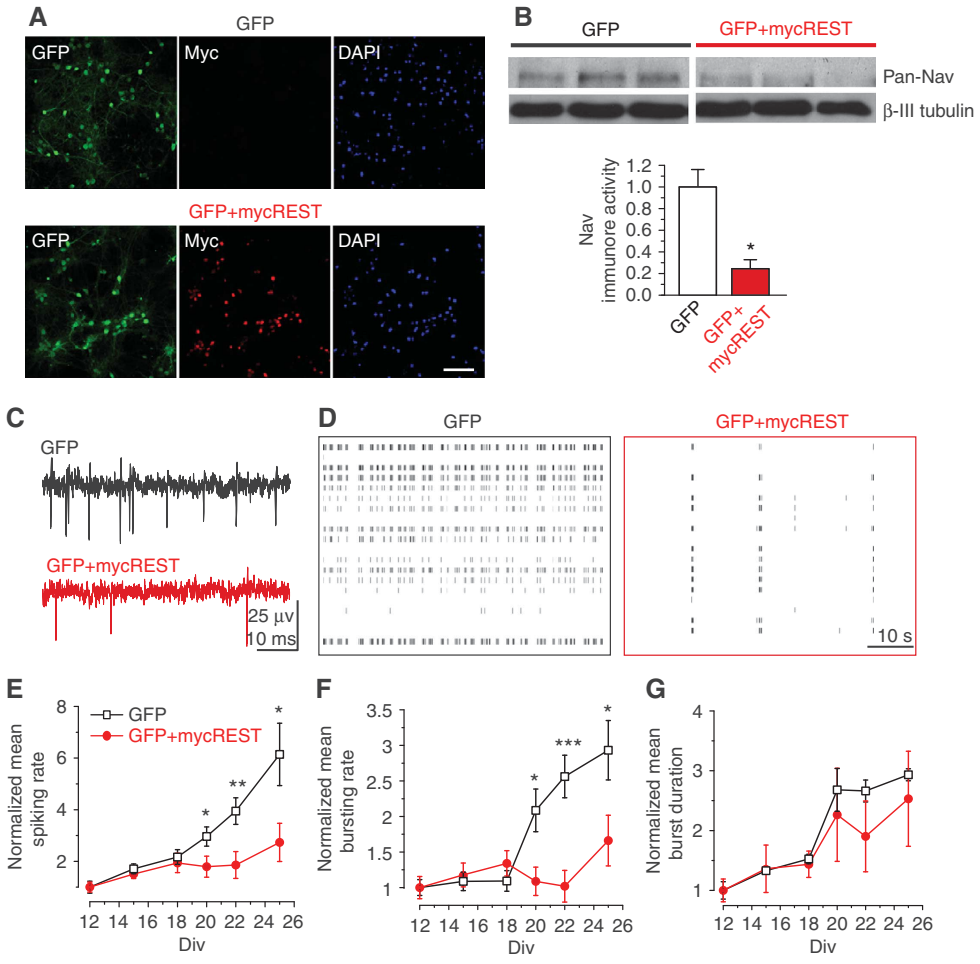

Figure 6 Overexpression of REST/NRSF downregulates VGNa channels and downscales the global firing activity of neuronal networks. (**A**) Representative microphotographs of hippocampal neurons (25 div) co-infected with GFP together with either an empty vector (GFP; *upper panels*) or GFP + mycREST (*lower panels*). From left to right: GFP fluorescence (green), myc immunoreactivity (red), and DAPI staining (blue). Scale bar: 100 µm. (**B**) Western blot analysis of neurons expressing either GFP or GFP + mycREST and stained with anti-Nav and β-III tubulin. The bar histogram represents the mean (± s.e.m.) normalized optical density for GFP- and GFP + mycREST-expressing neurons ($^*P<0.05$, unpaired two-tailed Student's *t*-test; $n=6$ from three independent culture preparations). (**C**, **D**) Representative voltage traces (**C**) and raster plots (**D**) of network activity for GFP- (black) and GFP + mycREST-expressing neurons (red) at 25 div. Small vertical bars in (**D**) represent single action potentials. (**E**–**G**) Spiking rate (**E**), bursting rate (**F**), and burst duration (**G**) measured in GFP- (black symbols; $n=14$) and GFP + mycREST- (red symbols; $n=13$) expressing neurons as a function of time *in vitro*. Data (means ± s.e.m.) were normalized to the respective values at 12 div. In GFP + mycREST-expressing neurons, a significant decrease in the spiking rate and in the bursting rate was observed ($^*P<0.05$, $^{**}P<0.01$, $^{***}P<0.001$, two-way ANOVA for repeated measurements followed by the Bonferroni's multiple comparisons test). Source data for this figure is available on the online supplementary information page.

(Figure 8E and F). In contrast, the cultures in which REST/NRSF had been knocked down by transduction with either shRNA#1 (Figure 8E) or shRNA#2 (Supplementary Figure S9) failed to scale down the initially increased neuronal firing activity and maintained high firing rates for up to 96 h. As already observed for REST/NRSF overexpression (see Figure 6F), the effects on the firing rate were entirely due to changes in bursting rate (Figure 8F) rather than in burst duration (Figure 8G). Taken together, these results demonstrate that the changes in endogeneous REST/NRSF levels induced by the activity of neuronal networks play a key role in the control of the global firing activity.

Discussion

Homeostatic plasticity, a fundamental process for the stabilization of central neuronal networks, has been shown to take place both during development (Burrone *et al*, 2002) and in the mature brain (Echegoyen *et al*, 2007). A synaptic involvement underlying homeostatic plasticity during sustained neuronal activity was shown to consist of coordinated changes at both the presynaptic (Murthy *et al*, 2001; Wilson *et al*, 2005; Moulder *et al*, 2006; Zhao *et al*, 2011) and the postsynaptic (Seeburg *et al*, 2008; Gainey *et al*, 2009; Beique *et al*, 2011; Hou *et al*, 2011) compartments. Although very effective, synaptic homeostasis is not the only means for scaling neuronal activity. An alternative and powerful mechanism is the modulation of the intrinsic excitability (Turrigiano, 2011) activated by changes in neuronal activity. In particular, long-term exposure to TTX produces a pattern of changes in voltage-dependent conductances characterized by an increase in VGNa current (Desai *et al*, 1999; Aptowicz *et al*, 2004) and a decrease in the persistent K^+ current (Desai *et al*, 1999). In contrast, an increase in neuronal activity was

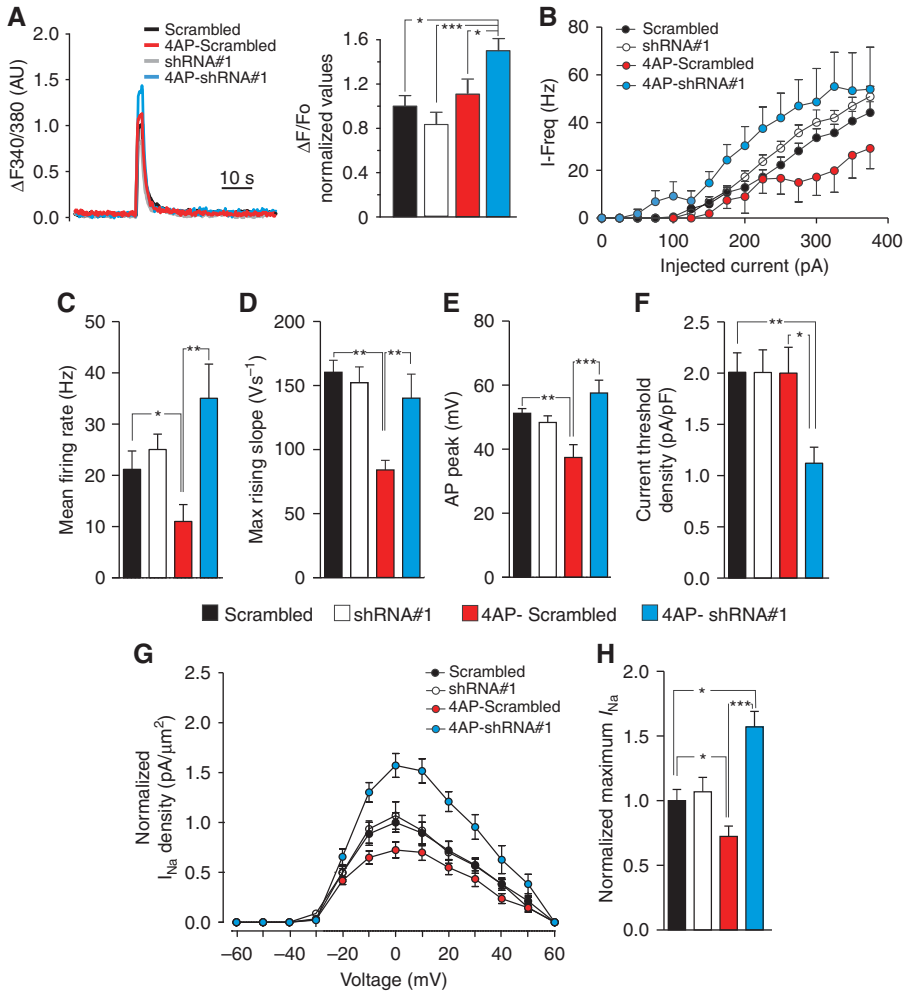

Figure 7 REST/NRSF controls intrinsic homeostasis induced by neuronal hyperactivity. (**A**) (*Left*) Representative electrically evoked Ca^{2+} transients measured at 18 div in neurons transfected with either scrambled shRNA (red trace/bar) or shRNA#1, exposed or not to 4AP for 96 h, as indicated. (*Right*) The bar histogram shows the amplitude of evoked Ca^{2+} transients (means ± s.e.m.) recorded in the four experimental groups. After 4AP treatment, neurons transfected with shRNA#1 ($n = 61$) showed significantly higher Ca^{2+} transients than neurons transfected with scrambled shRNA in the absence ($n = 27$) or presence ($n = 50$) of 4AP neurons or neurons transfected with shRNA#1 in the absence of 4AP ($n = 29$) (*$P < 0.05$, ***$P < 0.001$, one-way ANOVA followed by the Bonferroni's multiple comparison test). (**B**) Plots of the mean instantaneous frequency versus injected current (iF/I curve) in pyramidal neurons transfected with either scrambled shRNA or shRNA#1 and incubated for 96 h in the absence or presence of 4AP ($n = 11$–13 for each treatment). (**C**–**F**) Mean (± s.e.m.) firing rate (**C**), maximum rising slope (**D**), action potential peak (**E**), and current threshold density (**F**) under the conditions described above. (*$P < 0.05$, **$P < 0.01$, ***$P < 0.001$, one-way ANOVA followed by the Bonferroni's multiple comparison test). (**G**, **H**) Normalized I_{Na} density versus voltage plots (**G**) and normalized maximum amplitude measured at 0 mV (**H**) in pyramidal neurons transfected with either scrambled shRNA or shRNA#1 and incubated for 96 h in the absence or presence of 4AP ($n = 9$–12 for each treatment) (*$P < 0.05$, ***$P < 0.001$, one-way ANOVA followed by the Bonferroni's multiple comparisons test). Source data for this figure is available on the online supplementary information page.

reported to be associated with a reduction in intrinsic excitability (Karmarkar and Buonomano, 2006) due to an enhancement in the sub-threshold K^+ conductance (O'Leary *et al*, 2010). More recently, it has been demonstrated that, during 48 h of clamped depolarization with high KCl, the VGNa current of the axonal initial segment (AIS) undergoes relocation along the axon, thereby affecting neuronal excitability (Grubb and Burrone, 2010). However, the molecular mechanisms underlying such activity-dependent reorganization of membrane conductances, as well as their consequences on the overall activity of the neuronal networks, are still unexplored.

Here, we have investigated the effects on neuronal firing, $[Ca^{2+}]_i$ transients, VGNa currents and overall network activity triggered by a long-term treatment with a well-known stimulatory agent, the K^+ channel inhibitor 4AP. We found 4AP to be an appropriate agent for the induction of homeostatic plasticity. In fact, the hyperactivity induced by the drug, revealed by $[Ca^{2+}]_i$ rises and high firing rates 24 h after the beginning of the treatment, was greatly reduced after 48 h and virtually abolished after 96 h. Thus, the 4AP-induced stimulation was balanced by a complex of multifactorial inhibitory homeostatic responses, developing over time in the neuronal network.

Previous results have reported that the hyperexcitation-induced homeostatic plasticity would result from a synaptic downscaling occurring at both excitatory (Chang *et al*, 2010; Goold and Nicoll, 2010) and inhibitory synapses (Hartmann *et al*, 2008; Rannals and Kapur, 2011). Although several mechanisms might be at the basis of such complex event, we concentrated our study on the downregulation of the $VGNa^+$ channel-mediated intrinsic excitability of excitatory

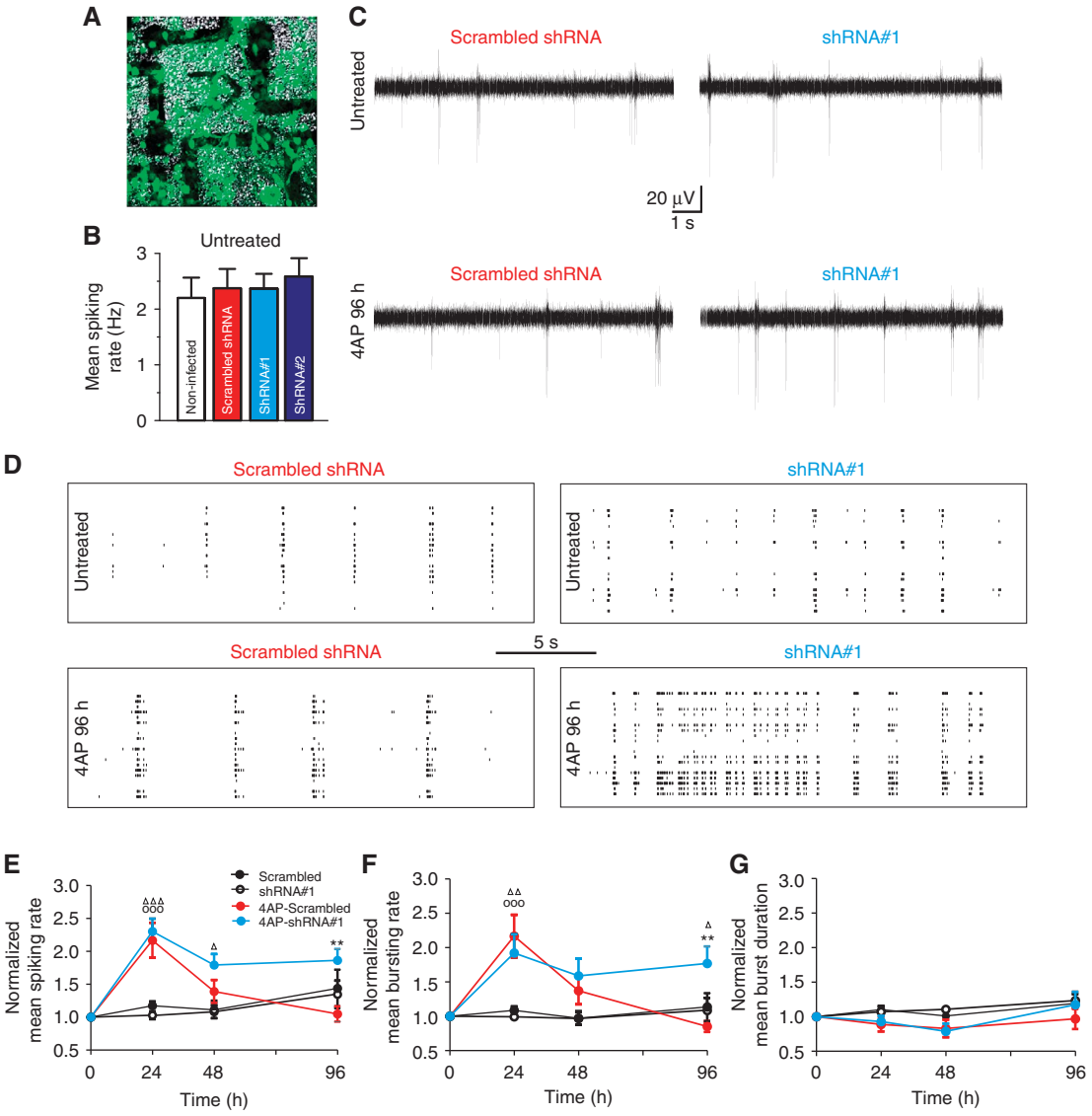

Figure 8 REST/NRSF-mediated homeostatic plasticity restores physiological excitability in the whole neuronal network. (**A**) Bright-field image of the MEA electrodes with a superimposed fluorescence image of neurons (20 div) infected with scrambled shRNA. (**B**) Untreated neuronal networks either non-infected (empty bar; $n = 11$) or infected at 14 div with scrambled shRNA (red bar; $n = 13$), shRNA#1 (light blue bar; $n = 12$) or shRNA#2 (blue bar; $n = 13$) showed similar mean firing rates at 20 div (means ± s.e.m.). (**C**) Representative voltage traces recorded from neurons transduced with either scrambled shRNA (left traces) or shRNA#1 (right traces) and incubated for 96 h in the absence (untreated; upper traces) or presence of 4AP for 96 h (4AP 96 h; lower traces). (**D**) Representative raster plots of network activity (20 channels) recorded from neurons transduced with either scrambled shRNA (left panels) or shRNA#1 (right panels) in the absence (untreated; upper panels) or presence of 4AP for 96 h (4AP 96 h, lower panels). (**E**–**G**) Mean (± s.e.m.) spiking rate (**E**), bursting rate (**F**), and burst duration (**G**) as a function of time in 4AP-treated or untreated cultures. Data were normalized with respect to the firing activity before the treatment (see **B**). ($^{\Delta}P<0.05$, $^{**}/^{\Delta\Delta}P<0.01$, $^{\Delta\Delta\Delta}/^{OOO}P<0.001$, two-way ANOVA for repeated measurements followed by the Bonferroni's multiple comparisons test. *4AP-Scrambled versus 4AP-shRNA#1; $^{\Delta}$Scrambled shRNA versus 4AP-shRNA#1; ^{O}Scrambled shRNA versus 4AP-Scrambled).

neurons because of its central role in governing network firing activity. Indeed, we found that firing rate, I_{Na} density, and VGNa channel expression were all strongly reduced by chronic 4AP treatment as compared to control conditions.

As Nav1.2 channels are major neuronal REST/NRSF targets (Chong *et al*, 1995; Schoenherr and Anderson, 1995a) and are downregulated in response to an increase in REST/NRSF expression (Nadeau and Lester, 2002), we hypothesized that the decreased neuronal excitability induced by the long-term 4AP treatment could be the consequence of an activity-dependent increase in REST/NRSF expression. REST/NRSF, initially identified as a master factor of neuronal specification during development (Chong *et al*, 1995; Schoenherr and Anderson, 1995b; Ballas and Mandel, 2005; Rodenas-Ruano *et al*, 2012), has been extensively investigated in neural cell lines such as PC12 cells (Bruce *et al*, 2006; D'Alessandro *et al*, 2008). Increases from the low REST/NRSF levels typical of mature neurons occurring during long-term stimulation with the glutamate analogue kainate (Palm *et al*, 1998; Spencer *et al*, 2006) or upon ischaemic insults (Calderone *et al*, 2003; Formisano *et al*, 2007) were reported to be critical for the induction of neuronal death. In contrast, we found that the increases in

REST/NRSF levels observed upon long-term treatment with 4AP do not lead to neuronal death. While REST/NRSF mRNA showed a transient increase, REST/NRSF protein was still upregulated after 96 h of 4AP incubation. The different temporal profile, likely due to feedback mechanisms restoring resting state REST/NSRF transcription and/or due to the longer half-life of REST/NSRF protein with respect to its mRNA, suggests that the transient activity-dependent modulation of REST/NRSF and Nav1.2 mRNA is sufficient to trigger a long-lasting homeostatic response.

The increase in REST/NRSF expression is fundamental for the establishment of a negative homeostatic response at both single-neuron and network levels. In fact, the effects of REST/NRSF overexpression largely phenocopied those obtained with long-term 4AP treatment. Although qualitatively similar, these two conditions are not quantitatively identical. Indeed, the increase in REST/NRSF expression levels induced by exogeneous overexpression is larger with respect to the endogeneous upregulation observed upon 4AP stimulation. Furthermore, it is known that RE-1 sequences located in the promoter region of several REST/NRSF target genes may vary considerably in number of repeats and REST/NRSF binding affinity (Bruce *et al*, 2004, 2009). Hence, the higher REST/NRSF levels achieved by exogeneous expression could induce the repression of other target genes with lower affinity for REST/NRSF, which are not modulated by 4AP treatment. Moreover, 4AP-mediated hyperactivity might activate a plethora of activity-dependent plasticity processes independent of REST/NRSF, with the involvement of multiple ion channels or proteins responsible for the control of neuronal excitability. Indeed, another transcriptional repressor, MeCP2, recruited to the same REST-RE1 site by CoREST (Ballas and Mandel, 2005), was recently reported to participate in the synaptic scaling up (Blackman *et al*, 2012) and scaling down (Zhong *et al*, 2012) in response to altered activity of neuronal circuits. However, the silencing of endogeneous REST/NRSF during chronic 4AP stimulation markedly impaired the homeostatic response observed in excitatory neurons, demonstrating a strong causal link between high REST/NRSF levels and the 4AP-triggered downregulation of intrinsic excitability through a reduction in I_{Na} and *Nav1.2* expression.

Recently, it has been demonstrated that Nav1.2 channels are located at the soma and at the proximal region of the AIS, whereas Nav1.6 channels preferentially accumulate at the distal end of the AIS, which represents the site for action potential initiation (Hu *et al*, 2009). This observation, together with the higher half-activation voltage of Nav1.2 channels with respect to Nav1.6 channels (Rush *et al*, 2005), can explain why the reduced expression of Nav1.2, evoked by 4AP treatment, decreases the action potential peak, maximum rising slope and instantaneous firing frequency, but leaves the voltage and current thresholds unaffected. However, hundreds of genes are known to be REST/NRSF targets in addition to the Nav1.2 channels (Chong *et al*, 1995; Schoenherr and Anderson, 1995a; Bruce *et al*, 2004; Johnson *et al*, 2007) and many of them code for channel proteins. Thus, the possibility that other channels are involved in the homeostatic response to 4AP stimulation cannot be ruled out.

The information provided here is also relevant for the field of epilepsy, in which the role of REST/NRSF is highly debated. The studies that identified the increase in REST/NRSF levels induced by kainic acid or ischaemia (a condition that induces an uncontrolled release of endogeneous glutamate) as a factor favouring neuronal death also indicated that REST/NRSF plays a pathogenic role in the appearance of the disease (Palm *et al*, 1998; Calderone *et al*, 2003; Spencer *et al*, 2006; Formisano *et al*, 2007; Noh *et al*, 2012). Results apparently consistent with this possibility were reported in nociceptive neurons of spinal ganglia, where increases in REST/NRSF were shown to increase the excitability (Mucha *et al*, 2010). Moreover, in kainate-induced *status epilepticus,* the increased REST/NRSF levels were reported to reduce the expression of the hyperpolarization-activated cyclic nucleotide-gated channel HCN1, making mice more vulnerable to seizures (McClelland *et al*, 2011). In other studies, however, REST/NRSF was reported to play an antiepileptic effect through the reduced expression of BDNF (Garriga-Canut *et al*, 2006). Such a potential protective role of REST/NRSF during epileptic-like neuronal activity has been recently reinforced by the observation that the conditional deletion of REST/NRSF dramatically accelerates seizure progression in the kindling model of epileptogenesis (Hu *et al*, 2011). Thus, the increased REST/NSRF levels associated with pathological conditions of hyperexcitability could be the expression of an endogeneous homeostatic, compensatory response rather than have a pathogenic role in the progression of the disease.

We have shown for the first time that the increased expression of REST/NRSF induced by neuronal hyperexcitation can reduce VGNa channel expression, downregulating I_{Na} at the single-cell level and reducing neuronal excitability and the overall neuronal network firing activity. In contrast, the levels of endogeneous REST/NRSF do not seem to be critical for the control of neuronal excitability under resting conditions and in the progressive increase of network activity during *in vitro* development. Despite the similar increases in REST/NRSF expression observed both upon sustained 4AP stimulation and during network development, 4AP might positively alter the expression/activity of other REST/NRSF cofactors, potentiating REST/NRSF-dependent transcriptional repression. Further studies are needed to better clarify this point.

In conclusion, although REST/NRSF is known to regulate the expression of many other genes that may also contribute to other homeostatic responses, possibly involving a scaling of synaptic efficiency, the transcriptional repression of VGNa channels by REST/NRSF appears to be one of the mechanisms governing the homeostatic response engaged by hyperactivity. Taken together, the data demonstrate a novel function of REST/NRSF in the physiology of mature neurons, going beyond its well-known role as a master regulation of neuronal differentiation.

Materials and methods

Cell cultures, transfection, and 4AP treatments

Hippocampal and cortical cultures were prepared from mouse C57BL/6J (E17–E18) embryos as previously described (Baldelli *et al*, 2007).

Patch-clamp recordings

Neuronal firing activity was studied by whole-cell current-clamp recordings and Na^+ current density was measured by macropatch

cell-attached voltage-clamp recordings. All current-clamp and macro-patch experiments were performed on morphologically identified pyramidal neurons by the teardrop-shaped somata and the presence of an apical-like dendrite (Watt *et al*, 2000; Pratt *et al*, 2003), which resulted GABA negative in retrospective immunocytochemistry analysis. Both approaches were performed using a Multiclamp 700B amplifier (Axon Instruments, Molecular Devices, Sunnyvale, CA, USA) using an upright BX51WI microscope (Olympus, Japan) equipped with Nomarski optics. The age of the patched neurons ranged between 14 and 16 div. Patch electrodes, fabricated from thick borosilicate glasses were pulled and fire-polished to a final resistance of 5–7 MΩ (for whole-cell configuration) or 1.5–2 MΩ (for macro-patch cell-attached configuration). Recordings with either leak currents >100 pA or series resistance >15 MΩ were discarded. Experiments were performed at 22–24°C. Macro-patch experiments and current-clamp recordings aimed at investigating single-cell firing rate were acquired at 10 kHz and low-pass filtered at 2 kHz. While the action potential shape was studied with a sampling frequency of 50 KHz and low-pass filtered at 10 kHz.

Action potentials were recorded in Tyrode extracellular solution to which D-(−)-2-amino-5-phosphonopentanoic acid (D-AP5; 50 μM), 6-cyano-7-nitroquinoxaline-2,3-dione (CNQX; 10 μM) and bicuculline methiodide (30 μM) were added to block NMDA, non-NMDA, and GABAA receptors, respectively. The internal solution (K gluconate) contained (in mM) 126 K gluconate, 4 NaCl, 1 $MgSO_4$, 0.02 $CaCl_2$, 0.1 BAPTA, 15 Glucose, 5 Hepes, 3 ATP, 0.1 GTP, pH 7.3. Only cells with resting membrane potentials between −57 and −64 mV were considered for analysis. Current-clamp recordings were performed at a holding potential of −70 mV, and action potential firing was induced by injecting current steps of 25 pA lasting 1000 ms. Instantaneous frequency (I-Freq.) was calculated between the first two evoked action potentials for each step.

The parameters describing the action potential shape were analysed using the pClamp software (Molecular Devices) and the Prism software (GraphPad Software, Inc.). For each recorded cell, the plot of the time derivative of voltage (dV/dt) versus voltage, called phase-plane plot, was obtained starting from the first action potential elicited by the minimal current injection (5 pA current steps). This parameter was used to better identify the voltage threshold and the maximum rising and repolarizing slopes (Bean, 2007). The voltage threshold was defined as the first voltage value at which dV/dt exceeded 10 mV/ms. The current threshold density was calculated as the minimum depolarizing current needed to elicit at least one action potential, divided by the cell capacitance.

Na^+ current density was measured as previously described (Magistretti *et al*, 1999) with the internal pipette solution containing (in mM) 130 NaCl, 35 TEA-Cl, 10 Hepes, 2 $CaCl_2$, 2 $MgCl_2$, 5 4AP, pH 7.4. Briefly, once the cell-attached configuration was obtained, the extracellular solution was rapidly switched to a high-potassium solution containing (in mM) 140 K acetate, 5 NaCl, 10 Hepes, 4 $MgCl_2$, 0.2 $CdCl_2$, 25 Glucose, pH 7.4. The holding potential was set at −100 mV. Na^+ currents were evoked by step depolarizations of 50 ms to a variable potential from −60 to +40 mV in 10 mV increments. Non-compensated capacitive currents were further reduced by subtracting averaged blank traces. The area of the patched membrane was estimated by measuring the pipette tip area. The Na^+ current density was obtained by dividing the peak inward current by the area of the patched membrane. Activation curves were obtained by plotting membrane potential steps versus Na^+ current amplitudes normalized to the maximum peak current. Inactivation curves were measured from a holding potential of −100 mV by depolarizing cells for 500 ms from −100 to −10 mV in 10 mV steps followed by 50 ms test pulses to −10 mV. Peak Na^+ currents were normalized to first peak current.

MEA recordings

Dissociated hippocampal neurons were plated onto 12-well planar Multi Electrode Arrays (Maestro 768-GL1-30Au200 from Axion Biosystems). These multi-electrode arrays consist of 768 electrodes segregated in 12 wells (64 electrodes/well), allowing for simultaneous extracellular recordings from different cultures. The electrode diameter was 30 μm, and the orthogonal distance between electrodes was 200 μm. The active electrode area was coated with poly-D-lysine (0.1 mg/ml, Sigma-Aldrich) and laminin (5 μl/ml, Sigma-Aldrich). Raw electrode data were digitized at 12.5 kHz and stored on a hard disk for further off-line analysis. For the developmental studies in neuronal cultures, extracellularly detected spontaneous action potential activity was recorded in Neurobasal solution for at least 20 min at 36.5°C, every 2 or 3 days from 12 to 25 div. Infection of the neuronal cultures was performed on 12 div after recordings of basal activity. The activity of the neuronal network was monitored in the absence and presence of 4AP added for 24, 48, or 96 h and data were normalized for the respective basal value recorded before the 4AP treatment. In these experiments, neuronal cultures were infected with shRNAs at 14 div and recorded from 20 to 24 div.

Spike detection was performed using a voltage-threshold-based algorithm run over 200 Hz high-pass-filtered traces; the voltage threshold was six-fold the standard deviation of the noise, whereas the refractory period was set to 2 ms. Spike train data were analysed using the Neuroexplorer software (Plexon). Bursts were identified by using the burst analysis algorithm of Neuroexplorer which reflects the following criteria: 100 ms maximum inter-spike interval to include a spike in a burst, 10 ms minimum burst duration and a minimum of 5 spikes/burst, as previously described (Vajda *et al*, 2008).

Calcium imaging and cell-death assays

Hippocampal neurons were loaded with Oregon Green-488 BAPTA-1, AM (3 μM) or Fura-2, AM (5 μM) (Molecular Probes) for 1 h at 37°C, 5% CO_2 in Neurobasal medium. Coverslips were mounted on a stimulation chamber (volume ∼100 μl; Warner Instruments, Hamden, CT) on the stage of an IX-71 inverted microscope (Olympus, Hamburg, Germany) equipped with a monochromator (Polychrome V, TILL Photonics). Cultures were imaged in extracellular Tyrode solution containing (in mM) 2 $CaCl_2$, 140 NaCl, 1 $MgCl_2$, 10 HEPES, 4 KCl, 10 glucose, pH 7.3, 300 mOsm, by using a cooled CCD camera (*ANDOR*, iXon 897) and sampling at 1 Hz with a ×40 objective (0.95 NA). The off-line analysis was performed with the TILL-vision software. Neurons were identified in bright field with differential interference contrast (DIC), and regions of interest (ROIs) of a 40-pixel area were drawn on the cell body. Ca^{2+} transients were measured as ΔF with respect to the baseline (F_0). Spontaneous activity was monitored for 5 min under resting conditions and in neurons treated for 24, 48, or 96 h with 4AP (100 μM) or vehicle. Data were normalized to untreated control cultures recorded at the same developmental stage. Evoked intracellular Ca^{2+} transients were induced by using field stimulation with 40 stimuli (duration: 0.5 ms; amplitude: 20 mA) delivered at 20 Hz.

For cell-death assays, hippocampal cultures were loaded with propidium iodide (Sigma) and Hoechst 33342 (Invitrogen) in Neurobasal medium for 20 min at 37°C and 5% CO_2. The percent cell death was determined from the ratio of propidium iodide-stained cells to the total number of Hoechst-stained cells.

Statistical analysis

The statistical analysis is presented in the figure legends. Data are given as means ± s.e.m. for n = sample size. The normal distribution of experimental data was assessed using D'Agostino-Pearson's normality test. The *F*-test was used to compare variance between two sample groups. To compare two normally distributed sample groups, the Student's unpaired two-tailed *t*-test was used, with Welch's correction applied in case the variance of the two groups was different. To compare two sample groups that were not normally distributed, we used Mann–Whitney's non-parametric *U* test. To compare more than two normally distributed sample groups, we used one- or two-way ANOVA, followed by either the Bonferroni's or the Dunnett's test. In cases in which data were not normally distributed, one-way ANOVA and two-way ANOVA were substituted with the Kruskal–Wallis's and Friedman's two-way ANOVA tests, respectively, followed by the Dunn's *post-hoc* multiple comparison test. Alpha levels for all tests were 0.5% (95% confidence intervals). Exact values of statistical significance for all experimental data are reported in Supplementary Table S2. Statistical analysis was carried out by using the SPSS (version 21, IBM Software) and the Prism software (GraphPad Software, Inc.).

Supplementary data

Supplementary data are available at *The EMBO Journal* Online (http://www.embojournal.org).

Acknowledgements

This study was supported by research grants from the Italian Ministry of University and Research (Progetti di Rilevante Interesse Nazionale to FB and FV); the Italian Ministry of Health Progetto Giovani (to PB); the Compagnia di San Paolo, Torino (to PB, FB, AF and FV); and the FET Proactive 7 Project (Grant EU 270483 to FB). The support of Telethon-Italy (Grant GGP09066 to PB and JM; Grant GGP09134 to FB and FV) is also acknowledged. We thank: Drs Luigi Naldini and Mario Amendola (Tiget, Milano, Italy) for invaluable help in lentiviral production protocols, Drs Marina Nanni, Claudia Chiabrera (The Italian Institute of Technology, Genova, Italy) and Silvia Casagrande (University of Genova, Italy) for precious help with cell cultures, Dr Lucian Medrihan and Federico Pecoraro for useful discussion and Eleonora Ferroni for help with analysis.

Author contributions: DP, GL, EF, AC, FP, RD, PL, and DB performed research; DP, GL, EF, AC, and PB analysed the data; DP, GL, AF, FV, and JM discussed and co-wrote the paper; FB and PB designed research, planned the experiments and wrote the paper.

Conflict of interest

The authors declare that they have no conflict of interest.

References

Amendola M, Venneri MA, Biffi A, Vigna E, Naldini L (2005) Coordinate dual-gene transgenesis by lentiviral vectors carrying synthetic bidirectional promoters. *Nat Biotechnol* **23:** 108–116

Aptowicz CO, Kunkler PE, Kraig RP (2004) Homeostatic plasticity in hippocampal slice cultures involves changes in voltage-gated Na+ channel expression. *Brain Res* **998:** 155–163

Baldelli P, Fassio A, Valtorta F, Benfenati F (2007) Lack of synapsin I reduces the readily releasable pool of synaptic vesicles at central inhibitory synapses. *J Neurosci* **27:** 13520–13531

Ballas N, Battaglioli E, Atouf F, Andres ME, Chenoweth J, Anderson ME, Burger C, Moniwa M, Davie JR, Bowers WJ, Federoff HJ, Rose DW, Rosenfeld MG, Brehm P, Mandel G (2001) Regulation of neuronal traits by a novel transcriptional complex. *Neuron* **31:** 353–365

Ballas N, Mandel G (2005) The many faces of REST oversee epigenetic programming of neuronal genes. *Curr Opin Neurobiol* **15:** 500–506

Bean BP (2007) The action potential in mammalian central neurons. *Nat Rev Neurosci* **8:** 451–465

Beique JC, Na Y, Kuhl D, Worley PF, Huganir RL (2011) Arc-dependent synapse-specific homeostatic plasticity. *Proc Natl Acad Sci USA* **108:** 816–821

Blackman MP, Djukic B, Nelson SB, Turrigiano GG (2012) A critical and cell-autonomous role for MeCP2 in synaptic scaling up. *J Neurosci* **32:** 13529–13536

Bruce AW, Donaldson IJ, Wood IC, Yerbury SA, Sadowski MI, Chapman M, Gottgens B, Buckley NJ (2004) Genome-wide analysis of repressor element 1 silencing transcription factor/neuron-restrictive silencing factor (REST/NRSF) target genes. *Proc Natl Acad Sci USA* **101:** 10458–10463

Bruce AW, Krejci A, Ooi L, Deuchars J, Wood IC, Dolezal V, Buckley NJ (2006) The transcriptional repressor REST is a critical regulator of the neurosecretory phenotype. *J Neurochem* **98:** 1828–1840

Bruce AW, Lopez-Contreras AJ, Flicek P, Down TA, Dhami P, Dillon SC, Koch CM, Langford CF, Dunham I, Andrews RM, Vetrie D (2009) Functional diversity for REST (NRSF) is defined by in vivo binding affinity hierarchies at the DNA sequence level. *Genome Res* **19:** 994–1005

Burrone J, Murthy VN (2003) Synaptic gain control and homeostasis. *Curr Opin Neurobiol* **13:** 560–567

Burrone J, O'Byrne M, Murthy VN (2002) Multiple forms of synaptic plasticity triggered by selective suppression of activity in individual neurons. *Nature* **420:** 414–418

Calderone A, Jover T, Noh KM, Tanaka H, Yokota H, Lin Y, Grooms SY, Regis R, Bennett MV, Zukin RS (2003) Ischemic insults derepress the gene silencer REST in neurons destined to die. *J Neurosci* **23:** 2112–2121

Chang MC, Park JM, Pelkey KA, Grabenstatter HL, Xu D, Linden DJ, Sutula TP, McBain CJ, Worley PF (2010) Narp regulates homeostatic scaling of excitatory synapses on parvalbumin-expressing interneurons. *Nat Neurosci* **13:** 1090–1097

Chong JA, Tapia-Ramirez J, Kim S, Toledo-Aral JJ, Zheng Y, Boutros MC, Altshuller YM, Frohman MA, Kraner SD, Mandel G (1995) REST: a mammalian silencer protein that restricts sodium channel gene expression to neurons. *Cell* **80:** 949–957

D'Alessandro R, Klajn A, Meldolesi J (2009) Expression of dense-core vesicles and of their exocytosis are governed by the repressive transcription factor NRSF/REST. *Ann NY Acad Sci* **1152:** 194–200

D'Alessandro R, Klajn A, Stucchi L, Podini P, Malosio ML, Meldolesi J (2008) Expression of the neurosecretory process in PC12 cells is governed by REST. *J Neurochem* **105:** 1369–1383

Desai NS, Rutherford LC, Turrigiano GG (1999) Plasticity in the intrinsic excitability of cortical pyramidal neurons. *Nat Neurosci* **2:** 515–520

Echegoyen J, Neu A, Graber KD, Soltesz I (2007) Homeostatic plasticity studied using in vivo hippocampal activity-blockade: synaptic scaling, intrinsic plasticity and age-dependence. *PLoS One* **2:** e700

Formisano L, Noh KM, Miyawaki T, Mashiko T, Bennett MV, Zukin RS (2007) Ischemic insults promote epigenetic reprogramming of mu opioid receptor expression in hippocampal neurons. *Proc Natl Acad Sci USA* **104:** 4170–4175

Gainey MA, Hurvitz-Wolff JR, Lambo ME, Turrigiano GG (2009) Synaptic scaling requires the GluR2 subunit of the AMPA receptor. *J Neurosci* **29:** 6479–6489

Garriga-Canut M, Schoenike B, Qazi R, Bergendahl K, Daley TJ, Pfender RM, Morrison JF, Ockuly J, Stafstrom C, Sutula T, Roopra A (2006) 2-Deoxy-D-glucose reduces epilepsy progression by NRSF-CtBP-dependent metabolic regulation of chromatin structure. *Nat Neurosci* **9:** 1382–1387

Goold CP, Nicoll RA (2010) Single-cell optogenetic excitation drives homeostatic synaptic depression. *Neuron* **68:** 512–528

Grubb MS, Burrone J (2010) Activity-dependent relocation of the axon initial segment fine-tunes neuronal excitability. *Nature* **465:** 1070–1074

Hartmann K, Bruehl C, Golovko T, Draguhn A (2008) Fast homeostatic plasticity of inhibition via activity-dependent vesicular filling. *PLoS One* **3:** e2979

Henze DA, Buzsaki G (2001) Action potential threshold of hippocampal pyramidal cells in vivo is increased by recent spiking activity. *Neuroscience* **105:** 121–130

Hou Q, Gilbert J, Man HY (2011) Homeostatic regulation of AMPA receptor trafficking and degradation by light-controlled single-synaptic activation. *Neuron* **72:** 806–818

Hu W, Tian C, Li T, Yang M, Hou H, Shu Y (2009) Distinct contributions of Na(v)1.6 and Na(v)1.2 in action potential initiation and backpropagation. *Nat Neurosci* **12:** 996–1002

Hu XL, Cheng X, Cai L, Tan GH, Xu L, Feng XY, Lu TJ, Xiong H, Fei J, Xiong ZQ (2011) Conditional deletion of NRSF in forebrain neurons accelerates epileptogenesis in the kindling model. *Cereb Cortex* **21:** 2158–2165

Ivenshitz M, Segal M (2010) Neuronal density determines network connectivity and spontaneous activity in cultured hippocampus. *J Neurophysiol* **104:** 1052–1060

Johnson DS, Mortazavi A, Myers RM, Wold B (2007) Genome-wide mapping of in vivo protein-DNA interactions. *Science* **316:** 1497–1502

Karmarkar UR, Buonomano DV (2006) Different forms of homeostatic plasticity are engaged with distinct temporal profiles. *Eur J Neurosci* **23:** 1575–1584

Kuba H, Oichi Y, Ohmori H (2010) Presynaptic activity regulates Na(+) channel distribution at the axon initial segment. *Nature* **465:** 1075–1078

Magistretti J, Ragsdale DS, Alonso A (1999) High conductance sustained single-channel activity responsible for the low-thresh-

old persistent Na(+) current in entorhinal cortex neurons. *J Neurosci* **19:** 7334–7341

McClelland S, Flynn C, Dube C, Richichi C, Zha Q, Ghestem A, Esclapez M, Bernard C, Baram TZ (2011) Neuron-restrictive silencer factor-mediated hyperpolarization-activated cyclic nucleotide gated channelopathy in experimental temporal lobe epilepsy. *Ann Neurol* **70:** 454–464

Moulder KL, Meeks JP, Mennerick S (2006) Homeostatic regulation of glutamate release in response to depolarization. *Mol Neurobiol* **33:** 133–153

Mucha M, Ooi L, Linley JE, Mordaka P, Dalle C, Robertson B, Gamper N, Wood IC (2010) Transcriptional control of KCNQ channel genes and the regulation of neuronal excitability. *J Neurosci* **30:** 13235–13245

Murthy VN, Schikorski T, Stevens CF, Zhu Y (2001) Inactivity produces increases in neurotransmitter release and synapse size. *Neuron* **32:** 673–682

Nadeau H, Lester HA (2002) NRSF causes cAMP-sensitive suppression of sodium current in cultured hippocampal neurons. *J Neurophysiol* **88:** 409–421

Noh KM, Hwang JY, Follenzi A, Athanasiadou R, Miyawaki T, Greally JM, Bennett MV, Zukin RS (2012) Repressor element-1 silencing transcription factor (REST)-dependent epigenetic remodeling is critical to ischemia-induced neuronal death. *Proc Natl Acad Sci USA* **109:** E962–E971

O'Leary T, van Rossum MC, Wyllie DJ (2010) Homeostasis of intrinsic excitability in hippocampal neurones: dynamics and mechanism of the response to chronic depolarization. *J Physiol* **588:** 157–170

Ooi L, Wood IC (2007) Chromatin crosstalk in development and disease: lessons from REST. *Nat Rev Genet* **8:** 544–554

Palm K, Belluardo N, Metsis M, Timmusk T (1998) Neuronal expression of zinc finger transcription factor REST/NRSF/XBR gene. *J Neurosci* **18:** 1280–1296

Pozo K, Goda Y (2010) Unraveling mechanisms of homeostatic synaptic plasticity. *Neuron* **66:** 337–351

Pratt KG, Watt AJ, Griffith LC, Nelson SB, Turrigiano GG (2003) Activity-dependent remodeling of presynaptic inputs by postsynaptic expression of activated CaMKII. *Neuron* **39:** 269–281

Rannals MD, Kapur J (2011) Homeostatic strengthening of inhibitory synapses is mediated by the accumulation of GABA(A) receptors. *J Neurosci* **31:** 17701–17712

Rodenas-Ruano A, Chavez AE, Cossio MJ, Castillo PE, Zukin RS (2012) REST-dependent epigenetic remodeling promotes the developmental switch in synaptic NMDA receptors. *Nat Neurosci* **15:** 1382–1390

Rush AM, Dib-Hajj SD, Waxman SG (2005) Electrophysiological properties of two axonal sodium channels, Nav1.2 and Nav1.6, expressed in mouse spinal sensory neurones. *J Physiol* **564:** 803–815

Schmidt JW, Catterall WA (1986) Biosynthesis and processing of the alpha subunit of the voltage-sensitive sodium channel in rat brain neurons. *Cell* **46:** 437–444

Schoenherr CJ, Anderson DJ (1995a) The neuron-restrictive silencer factor (NRSF): a coordinate repressor of multiple neuron-specific genes. *Science* **267:** 1360–1363

Schoenherr CJ, Anderson DJ (1995b) Silencing is golden: negative regulation in the control of neuronal gene transcription. *Curr Opin Neurobiol* **5:** 566–571

Seeburg DP, Feliu-Mojer M, Gaiottino J, Pak DT, Sheng M (2008) Critical role of CDK5 and Polo-like kinase 2 in homeostatic synaptic plasticity during elevated activity. *Neuron* **58:** 571–583

Spencer EM, Chandler KE, Haddley K, Howard MR, Hughes D, Belyaev ND, Coulson JM, Stewart JP, Buckley NJ, Kipar A, Walker MC, Quinn JP (2006) Regulation and role of REST and REST4 variants in modulation of gene expression in in vivo and in vitro in epilepsy models. *Neurobiol Dis* **24:** 41–52

Tomasoni R, Negrini S, Fiordaliso S, Klajn A, Tkatch T, Mondino A, Meldolesi J, D'Alessandro R (2011) A signaling loop of REST, TSC2 and beta-catenin governs proliferation and function of PC12 neural cells. *J Cell Sci* **124:** 3174–3186

Turrigiano G (2011) Too many cooks? Intrinsic and synaptic homeostatic mechanisms in cortical circuit refinement. *Annu Rev Neurosci* **34:** 89–103

Turrigiano GG (2008) The self-tuning neuron: synaptic scaling of excitatory synapses. *Cell* **135:** 422–435

Vajda I, van Pelt J, Wolters P, Chiappalone M, Martinoia S, van Someren E, van Ooyen A (2008) Low-frequency stimulation induces stable transitions in stereotypical activity in cortical networks. *Biophys J* **94:** 5028–5039

Watt AJ, van Rossum MC, MacLeod KM, Nelson SB, Turrigiano GG (2000) Activity coregulates quantal AMPA and NMDA currents at neocortical synapses. *Neuron* **26:** 659–670

Wilson NR, Kang J, Hueske EV, Leung T, Varoqui H, Murnick JG, Erickson JD, Liu G (2005) Presynaptic regulation of quantal size by the vesicular glutamate transporter VGLUT1. *J Neurosci* **25:** 6221–6234

Zhao C, Dreosti E, Lagnado L (2011) Homeostatic synaptic plasticity through changes in presynaptic calcium influx. *J Neurosci* **31:** 7492–7496

Zhong X, Li H, Chang Q (2012) MeCP2 Phosphorylation Is Required for Modulating Synaptic Scaling through mGluR5. *J Neurosci* **32:** 12841–12847